Neutron Stimulated Emission Computed Tomography for Diagnosis of Breast Cancer

Anuj J. Kapadia, Amy C. Sharma, Georgia D. Tourassi, Janelle E. Bender, Calvin R. Howell, Alexander S. Crowell, Matthew R. Kiser, Brian P. Harrawood, Ronald S. Pedroni, and Carey E. Floyd, Jr.

***Abstract*—Neutron stimulated emission computed tomography (NSECT) is being developed as a non-invasive spectroscopic imaging technique to determine element concentrations in the human body. NSECT uses a beam of fast neutrons that scatter inelastically from atomic nuclei in tissue, causing them to emit characteristic gamma photons that are detected and identified using an energy-sensitive gamma detector. By measuring the energy and number of emitted gamma photons, the system can determine the elemental composition of the target tissue. Such determination is useful in detecting several disorders in the human body that are characterized by changes in element concentration, such as breast cancer. In this paper we describe our experimental implementation of a prototype NSECT system for the diagnosis of breast cancer and present experimental results from sensitivity studies using this prototype. Results are shown from three sets of samples: (a) excised breast tissue samples with unknown element concentrations, (b) a multi-element calibration sample used for sensitivity studies, and (c) a small-animal specimen, to demonstrate detection ability from *in-vivo* tissue. Preliminary results show that NSECT has the potential to detect elements in breast tissue. Several elements were identified common to both benign and malignant samples, which were confirmed through neutron activation analysis (NAA). Statistically significant differences were seen for peaks at energies corresponding to ^{37}Cl, ^{56}Fe, ^{58}Ni, ^{59}Co, ^{66}Zn, ^{79}Br and ^{87}Rb. The spectrum from the small animal specimen showed the presence of ^{12}C from tissue, ^{40}Ca from bone, and elements ^{39}K, ^{27}Al, ^{37}Cl, ^{56}Fe, ^{68}Zn and ^{25}Mg. Threshold sensitivity for the four elements analyzed was found to range from 0.3 grams to 1 gram, which is higher than the microgram sensitivity required for cancer detection. Patient dose levels from NSECT were found to be comparable to those of screening mammography.**

***Index Terms*—Breast cancer detection, gamma-ray spectroscopy, neutron, NSECT, tomography.**

Manuscript received January 5, 2007; revised July 2, 2007. This work was supported in part by the NIH/NCI under Grant 1-R21-CA106873-01, in part by the Department of Defense (Breast Cancer Research Program) under award number W81XWH-06-1-0484, and in part by the U.S. Department of Energy, Office of High Energy and Nuclear Physics under Grant DE-FG02-97ER41033.

A. J. Kapadia and A. C. Sharma are with the Department of Biomedical Engineering and the Duke Advanced Imaging Laboratories (DAILabs), Department of Radiology, Duke University, Durham, NC 27710 USA (e-mail: anuj.kapadia@duke.edu; anc4@duke.edu).

G. D. Tourassi and B. P. Harrawood are with the Duke Advanced Imaging Laboratories (DAILabs), Department of Radiology, Duke University, Durham, NC 27710 USA (e-mail: gt@deckard.duhs.duke.edu; brian.harrawood@duke.edu).

J. E. Bender is with the Department of Biomedical Engineering, Duke University, Durham, NC 27710 USA (e-mail: janelle.bender@duke.edu).

C. R. Howell, A. S. Crowell, and M. R. Kiser are with the Department of Physics, Duke University, Durham, NC 27710 USA and also with Triangle Universities Nuclear Laboratory, Durham, NC 27708 USA (e-mail: howell@tunl.duke.edu; crowell@tunl.duke.edu; kiser@tunl.duke.edu).

R. S. Pedroni is with the Department of Physics, North Carolina A&T State University, Greensboro, NC 27411 USA.

C. E. Floyd Jr. is with Duke Advanced Imaging Laboratories (DAILabs), Department of Radiology, Duke University Medical Center and also with the Department of Biomedical Engineering Duke University, Durham, NC 27710 USA.

Color versions of one or more of the figures in this paper are available online at http://ieeexplore.ieee.org.

Digital Object Identifier 10.1109/TNS.2007.909847

I. Introduction

NEUTRON techniques are rapidly evolving as methods of measuring trace element concentrations in the human body [1]–[6] and in animal tissue [7], [8]. We have successfully implemented a tomographic non-invasive *in-vivo* imaging technique called Neutron Stimulated Emission Computed Tomography (NSECT) to obtain two-dimensional tomographic information about element concentration within a target tissue sample [9]–[17]. NSECT uses spectral information obtained from inelastic scattering interactions between neutrons and atomic nuclei in the target sample to identify the target atoms and determine their concentration *in-vivo*.

Such a technique has several potential applications in both humans and small animals. Several studies have indicated that changes in trace element concentrations in human tissue may be a precursor to malignancy in several organs, for example, brain, prostate and breast [1], [5], [6], [18]–[20]. Measuring these concentration changes would provide the ability to differentiate between malignant and benign tissue, and their quantification could enable *in-vivo* cancer diagnosis at very early stages. Element concentration changes have also been observed in iron for diseases such as sickle cell anemia, thalassemia major, hemosiderosis and hemochromatosis [21]–[27], and in copper for Wilson's disease [28]. NSECT has the potential to image element concentrations in tomographic regions of interest within affected organs, which can help in diagnosis and management of these disorders.

The underlying NSECT principle is the following. NSECT relies on inelastic scattering interactions that occur when atomic nuclei are bombarded with fast neutrons. When an incident neutron scatters inelastically with a target atomic nucleus, the nucleus gets excited to one of its quantized higher-energy states which is often unstable. This excited nucleus then rapidly decays to a lower state, emitting a gamma ray photon whose energy is equal to the difference between the energies of the two states. These non-overlapping energy states are well established and somewhat unique to each element and isotope. Thus, detection and analysis of the emitted gamma energy spectrum can be used to identify the emitting target atom.

While the NSECT technique may seem somewhat similar to prompt gamma neutron activation analysis (PGNAA) as gamma rays emitted due to interactions with incident neutrons are measured simultaneously while irradiating the sample, the two techniques differ greatly in the method of gamma ray production. PGNAA relies on neutron capture with prompt gamma emission, while NSECT uses inelastic scatter spectroscopy to identify the scattering isotope without inducing radioactivity. The NSECT technique is a computed tomography extension of neutron inelastic scatter spectroscopy.

Emitted gamma photons are captured using an energy-sensitive gamma-ray detector. Tomography is performed by acquiring a complete set of projections of line integrals using the translate-rotate configuration as in first generation CT scanners, i.e. the beam is translated horizontally through the entire sample length, then the sample is rotated through some fixed angle and the process is repeated. This tomographic scanning technique yields a two-dimensional map of element concentration and distribution within the sample. This translate-rotate geometry is appropriate for initial proof of concept studies using phantoms, specimens or small animals. Once feasibility is demonstrated, other geometries can be used in future clinical systems. Images are reconstructed using the Maximum Likelihood Expectation Maximization algorithm, an iterative technique to optimize an image reconstructed from a finite set of its projections [29]–[31].

This manuscript presents NSECT as a potential application for diagnosis of breast cancer. Early detection has proven to be the most effective technique to increase survival rates of patients with breast cancer. While screening mammography has been proven to be effective in screening for breast cancer, it suffers from the following limitations: (a) it requires that the mammograms have good contrast, which is often difficult to achieve in dense breasts; (b) its anatomic approach in trying to identify abnormalities in mammograms makes it essential that the abnormality be in an advanced stage of development; and (c) it has limitations in classifying detected abnormalities as benign or malignant. NSECT's sensitivity to metabolic changes seen in malignant tumors in very early developmental stages has the potential to overcome the disadvantages of screening mammography.

Several studies have demonstrated that breast cancer is associated with changes in trace element concentration in the malignant tissue at very early stages. These changes have been observed in concentration of elements such as Al, Br, Ca, Cl, Co, Cs, Cu, Fe, K, Mn, Na, Rb, Sb, Se and Zn, and often occur much earlier than morphologic changes such as tumors and calcifications begin to appear [1], [6], [18]–[20], [32]. Quantifying these element concentrations could potentially enable diagnosis of breast cancer much before the tumor grows large enough to be detected by existing imaging techniques. Generally, NSECT's role in diagnosing breast cancer is to (i) spectroscopically quantify the concentration of elements of interest in the tissue to diagnose the disorder, and (ii) generate three dimensional tomographic image of the element concentration in the organ to isolate the region affected by the disorder. As most of these trace elements occur in the body in microgram quantities, a primary objective of this study is to determine whether NSECT has the required sensitivity to detect micro-gram concentration changes *in-vivo*.

In this paper we describe our experimental implementation of a prototype NSECT system for the diagnosis of breast cancer and present experimental results from sensitivity studies using this prototype. This manuscript presents the first results from a spectroscopic examination of the breast as a preliminary step in determining whether it is realistic to develop NSECT for diagnosis of breast cancer in a clinical scenario.

II. Materials and Methods

A. Description of NSECT Prototype System

NSECT experiments have been performed at the Triangle Universities Nuclear Laboratory (TUNL) accelerator lab located at Duke University. TUNL is a low energy nuclear physics research laboratory with a variety of ion beam sources and a 10 megavolt tandem Van de Graaff accelerator capable of producing 20 MeV proton or deuteron beams and a host of other light ion beams. The shielded neutron source provides researchers with an intense pulsed collimated mono-energetic neutron beam. The shape and cross sectional dimension of the beam can be selected with collimator inserts in the 1.5 meter thick shielding wall. For instance, beams with rectangular cross sections are available with sides ranging from 1 mm to 60 mm. The reduction in the background by the 1.5 meter thick wall is sufficient to permit gamma-ray detectors to be used without extensive shielding. The key NSECT components are described below.

1) Neutron Source: Neutrons are produced through the $^{2}\mathrm{H}(\mathrm{d},\mathrm{n})^{3}\mathrm{He}$ reaction by directing an accelerated and pulsed beam of deuterons onto a deuterium gas target. Deuterons are accelerated to energies between 3 and 20 MeV by the tandem Van de Graaff accelerator. The charged deuteron beam is directed onto a pressurized deuterium gas cell located behind a 1 meter thick shielding wall composed of concrete, steel, lead, and paraffin loaded with boron and lithium. Beam positioning and focusing on target are performed using magnetic steering coils and magnetic quadrupole lenses, respectively. A collimated channel made of copper with swappable inserts is used to select the beam profile. Copper is chosen because it adequately attenuates neutrons at energies available at TUNL, is fairly simple to machine and is reasonably low cost. For this experiment, the beam profile was selected to be cylindrical with 6 cm diameter.

The neutron beam created is highly peaked in the forward direction and has a narrow energy width of approximately 1 MeV. Neutron beam energies between 5 and 23.2 MeV are available at TUNL.

The beam is pulsed to provide 2 ns wide bunches at the target to allow measurement of neutron and gamma time of flight (TOF), enabling TOF background correction. The repetition rate of the beam pulses is adjustable from 2.5 MHz down to 39 kHz. This pulsed neutron beam allows researchers to measure the background simultaneously with the foreground.

2) Neutron Flux Monitors: After exiting the collimator channel, the beam is incident on a thin neutron flux monitor made of a 1.6 mm thick plastic scintillator attached to a

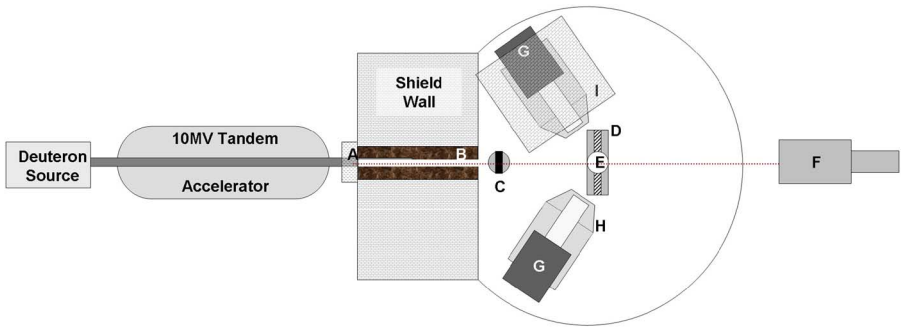

Fig. 1. Schematic drawing of the experimental setup used in NSECT measurements. Components are labeled as follows: A—Deuterium Gas Cell; B—Copper Collimator; C—Neutron Flux Monitor; D—Sample Manipulator; E—Sample; F—Zero-degree Liquid Scintillator Detector; G—HPGe detector; H—Anti-coincidence Compton Shield; I—Detector Shielding Enclosure.

photomultiplier tube. The attenuation of neutrons by the flux monitor in the energy range of our studies is less than 0.1%. The threshold setting on the discriminator of the flux monitor is set sufficiently high to reject more than 90% of the pulses due to recoil electrons from Compton scattering of gamma rays. The efficiency of the thin flux monitor is calibrated relative to a liquid scintillator detector positioned at 0 degrees with respect to the beam. This detector has an active volume 5 inches diameter $\times$ 0.74 inches thick and is filled with Bicron Corporation's BC519 scintillator fluid that enables gamma-ray rejection by pulse shape analysis. The absolute efficiency of this detector has been determined in a separate measurement to an accuracy of $\pm$5% [33]. The zero degree liquid scintillator detector is also used to obtain the neutron transmission image of the sample which is required to make attenuation corrections.

3) Sample Manipulator: A computer-controlled sample holder allows precise horizontal, vertical and rotational positioning of small samples remotely. This holder allows tomographic acquisition by translating and rotating the sample with respect to the neutron beam. In the current implementation, tomography is performed by using the translate-rotate geometry to obtain a complete set of projections of line integrals through a slice of the sample. For NSECT, these projections are defined by the angular and spatial sampling intervals between successive positions of the sample as positioned by the sample manipulator.

4) Gamma Detectors: Two high-purity germanium (HPGe) detectors are used to detect gamma rays emitted from the sample. These detectors are the 2-Fold Segmented Clover Detectors (CLOVER $4 \times 50 \times 80$ SEG2) manufactured by Canberra Eurysis S.A. Each detector consists of four co-axial n-type germanium crystals mounted together in the shape of a 4-leaf clover. Each germanium crystal is 50 mm in diameter and 80 mm in length, with minimum relative efficiency of 22% and full width at half maximum less than or equal to 2.25 keV for 1.332 MeV gamma rays of ^{60}Co. Both detectors were calibrated against known energy peaks from a ^{22}Na source and positioned at $\pm$135 degrees from the incident neutron beam at a distance of 20 cm from the sample. A majority of the states of interest decay by an electric quadrupole transition whose distribution has a maximum intensity at about 45 and 135 degrees. Using the 135 degree orientation helps prevent the gamma detector from being illuminated by either the direct neutron beam or by neutrons that elastically scatter from the target. Active Compton shielding is used to reduce the effects of Compton scattering in the detectors. These shields have a minimum peak-to-Compton ratio of 41 for ^{60}Co gamma rays at 1.332 MeV.

A schematic drawing of the source, detector and shielding configuration is shown in Fig. 1.

5) Passive Shielding: The gamma detector is shielded from the neutron source by a 1.5 m thick wall composed of concrete, steel, lead, borated plastic and lithium-loaded paraffin. In addition to this wall, an enclosure of lead bricks and lithium-loaded paraffin built around each detector provides additional shielding to further reduce particles incident on the active area of the detector.

6) Computers and Acquisition Software: Data is acquired using SpecTcl, a nuclear event data acquisition and analysis software package developed at the National Superconducting Cyclotron Laboratory at Michigan State University. SpecTcl allows acquisition and storage of raw data using an object oriented C++ framework, and allows online and offline data visualization through the Xamine display program. Complete as well as partial sets of raw data can be retrieved at any time, including during acquisition, and analyzed using any combination of data parameters. The Xamine display program allows simultaneous display of multiple spectra including spectrum overlay.

7) Amplifiers: Canberra 2026 spectroscopy amplifiers are used to integrate and shape the signals from the gamma detectors before they are digitized by peak-sensing ADC's at the data acquisition interface. Adjustable gain settings on these amplifiers allow 'zooming' in or out on a specific range of nuclear energy levels. For example, acquiring data for a gamma energy range of 0–2 MeV would require double the gain as that for 0–4 MeV. However, as the number of channels in the ADC is finite, focusing the entire range of the ADC into a smaller energy range gives better energy resolution in the measured gamma ray energy spectrum. This feature is important when looking for specific energy peaks from certain elements, which lie close to energy peaks from other elements, as in the case of iron (56Fe at 846.7 keV) and germanium (74Ge at 841.1 keV).

B. Spectral Acquisition Methodology

Spectral acquisition for samples was performed by using SpecTcl to digitize two measurable quantities for each gamma count observed: gamma TOF and gamma photon energy. For each data acquisition run, several quantities were counted

using scalars and recorded. These scalars include neutron flux, accelerator beam current and the zero-degree monitor counts. For tomography, the sample position was recorded by reading the sample manipulator's x,y,z positions at each projection as the sample was translated and rotated. Each projection was then analyzed separately and results were fed to the reconstruction algorithm. Data were recorded for each projection until a statistical accuracy of 95% was obtained.

Recorded data sets could be retrieved and analyzed in both real-time while acquiring data as well as at a later time for off-line analysis. Analysis parameters such as TOF windows and detector calibration bias were applied and adjusted in software to allow replaying the experiment with different windows for off-line optimization of these parameters. Spectra were generated using the Xamine display program with different combinations of timing and energy windows applied to the acquired data.

1) Background Reduction: Background reduction was performed to account for three contributing sources of background: time uncorrelated events via a TOF background suppression technique [34], [35], sample uncorrelated backgrounds that are time correlated by a sample-out scan subtraction [35], and polynomial curve-fitting of the residual background, i.e. the background that remains after the measured contributions are subtracted. [13]–[15]. The TOF suppression technique is used to correct for the time-uncorrelated backgrounds that are due mostly to gamma rays created and noise generated from the neutron interactions in the shielding material and target apparatus. This technique uses a pulsed neutron beam to allow selection of gamma rays which appear within the prompt peak that corresponds to the time of flight for a neutron from the source to the sample plus the time of flight for the subsequently emitted gamma from the sample to the detector. The remaining gamma rays are suppressed as 'background noise'. The time zero for the TOF measurement is set by using pulsing information from the deuteron beam to control a clock that measures the time of flight of the neutrons from the gas cell to the sample plus the time of flight of the emitted gamma rays from the sample to the detector. Our implementation of this technique has been described in detail elsewhere [35].

Background events that are due to processes that don't involve the sample are measured by acquiring data with the sample removed. Examples of such processes are interactions of neutrons with the collimator or sample holder. This data is subtracted from the sample-in data to produce an estimate of the spectrum due to neutron interactions in the sample. This technique has been described in detail elsewhere [35]. In this study, the samples of interest were only the elements present in the tissue. Hence, the sample-out scan was acquired by substituting the tissue sample with an equivalent mass of water, i.e. removing only the elements of interest while retaining the neutron scatter properties of hydrogen and oxygen nuclei in tissue.

Polynomial curve fitting is used to remove residual background due to Compton scattering of detected gammas. When high energy gamma photons are incident on a detector, some of the gammas will deposit their full energy in the detector while others will scatter out of the detector active volume. As a result, there is a trend of increasing counts in the lower energy channels of the detector. A polynomial curve-fit is used to model this trend and subtract this residual background.

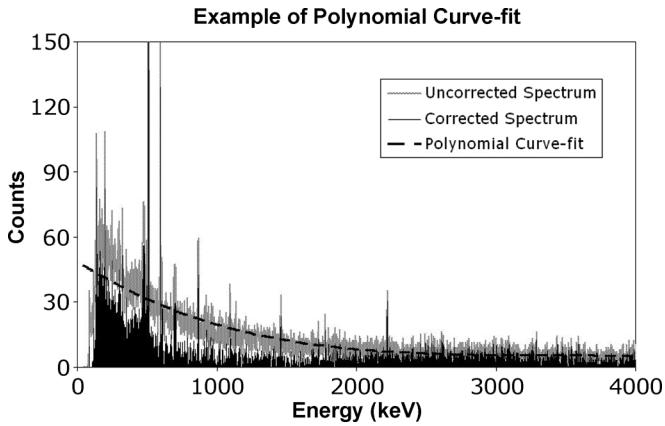

Fig. 2. Example of polynomial curve-fitting for residual background correction. The uncorrected spectrum is shown in grey with the polynomial curve overlaid in dotted black. The resulting corrected spectrum is shown in the foreground as a solid black line in the lower part of the image.

An example of this is shown in Fig. 2, which shows an original uncorrected spectrum (light gray), the polynomial curve fit to underlying background (dotted black line), and the spectrum after residual background correction (solid black line in the lower part of the image).

2) Samples: A total of 5 samples were scanned for this study investigating our ability to use NSECT to detect element concentration changes in human tissue. Samples I and II comprised breast biopsy tissue samples with matched tumors excised from the same patient. Sample I had a benign tumor and Sample II was malignant. Each sample weighed approximately 40 g and was scanned with a 6.0 MeV neutron beam while placed in a plastic container, delivering an integrated dose of approximately 1 mSv. Sample III comprised 40 g of distilled water in an identical plastic container, and was used to get an estimate of sample related background originating mainly from hydrogen and oxygen nuclei in tissue cells. Sample IV was made of varying concentrations of ^{56}Fe, ^{23}Na, ^{39}K, ^{35}Cl and ^{37}Cl in distilled water and was used as a calibration sample to determine the lower detection threshold of NSECT. Finally, as none of the above samples were of *in-vivo* tissue, Sample V comprising a fixed mouse specimen was scanned to demonstrate NSECT's ability in detecting elements from an intact biological specimen. The mouse specimen was prepared as follows. A freshly sacrificed mouse was flushed with saline and then fixed for one week using a 1:10 gadolinium/formalin solution. After flushing the fixed mouse with saline once again, it was enclosed and sealed in a glass tube along with diluted formalin solution. This enclosed specimen was scanned for 95 minutes with a 5.0 MeV monochromatic neutron beam.

Gamma spectra obtained from each sample were normalized against neutron flux monitor counts for the duration of the scan and corrected for sample uncorrelated backgrounds.

C. Spectral Analysis Methodology

After correcting for sample uncorrelated backgrounds, each spectrum was analyzed to identify the location of a peak using an automated peak-finding algorithm. The algorithm identifies a peak as a region of high intensity within a pre-specified energy window and peak height above a certain pre-specified threshold [36]. For the breast spectra in this experiment, the energy window width was defined as ± 10 keV and peak height threshold was set to 7. Each detected peak was compared to its underlying background using a z-score test for difference of means. Collection of gamma rays in the detectors is assumed to follow Poisson counting statistics, where, for each energy peak, the mean and variance are equal to the number of counts in the peak. With this assumption, the statistical significance for any two energy peaks can be calculated using the z-score test for a difference of means. Peaks with a two-tailed p-value ≤ 0.05 are considered significant. For each energy peak in the spectrum, an underlying background was calculated using a polynomial curve-fit as described earlier. The significance of the energy peak was determined by calculating the value of z as shown in (1), comparing the counts in the energy peak against counts in the underlying background

$$z = \frac{\mu_{peak} - \mu_{background}}{\sqrt{\mu_{peak} + \mu_{background}}}. \tag{1}$$

Only peaks detected with a 95% confidence level (i.e., two-tailed p-value ≤ 0.05) were reported for element matching. This analysis was performed separately for the benign and malignant breast spectra.

Each reported peak was then matched with potential elements using the National Nuclear Data Center's Nuclear structure and decay data online tool (NuDat 2.3) [37]. This identification was made in three steps: (a) a list of all elements with gamma lines at the energy peak of interest were listed; (b) isotopes of elements not expected to be present in the breast, including radioactive isotopes and stable isotopes with low abundance, were discarded from the list; (c) prior information about the remaining isotopes' line contributions to prominent gamma lines was used to identify a possible element match. Several elements such as ^{12}C, ^{40}Ca, ^{35}Cl ^{63}Cu, ^{56}Fe and, ^{16}O, which are present in the breast, have been scanned and studied in earlier NSECT experiments where several of these elements were scanned individually [9]–[11]. These individual element scans were used to experimentally establish the relative contribution of prominent gamma lines for each of these elements. This prior information was used in identifying the corresponding element in the breast spectra. However, there are many other elements in the breast spectrum that have not yet been scanned individually, and their contributions to different gamma lines have not been experimentally established. As a result, certain gamma energy peaks in the breast spectra were found to have multiple element matches, and these are labeled accordingly.

After identifying energy peaks in the individual spectrum, a z-score test for the difference of means was used to analyze the comparative differences in peak heights between the benign and malignant spectra. Counts in an energy peak identified as a potential element peak in a benign spectrum were compared to counts from the same energy peak in the malignant spectrum using the formula in (1). Each peak was considered individually for this analysis. Energy peaks that differed from each other at the 95% confidence level (i.e. two-tailed p-value ≤ 0.05) were reported as possible markers for malignancy.

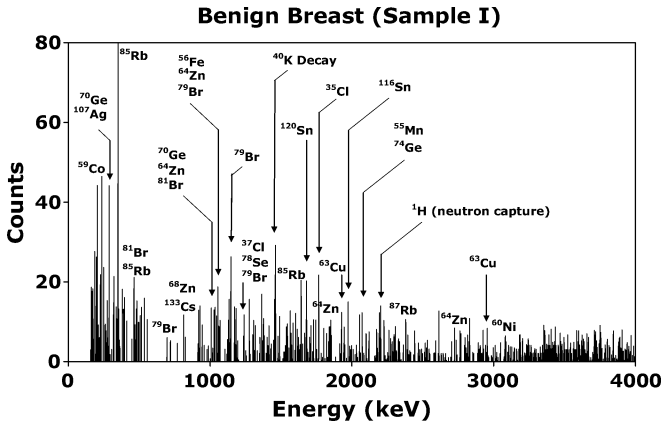

Fig. 3. Gamma energy spectrum from benign breast sample showing energy peaks for several potential elements identified. Gamma peaks are seen for ^{72}Ge and ^{74}Ge from the germanium detector. Peaks with multiple potential element matches are labeled accordingly.

For the multi-element calibration sample, prominent peaks corresponding to ^{56}Fe, ^{39}K, ^{23}Na and ^{35}Cl were identified in the spectrum, taking into consideration prior information about their line contributions to the peaks, and the intensity of their peaks was associated with the known concentration of the element in the sample. Assuming the statistical noise in the system to remain constant, threshold sensitivity for each element was calculated as the concentration at which the resulting peak could be detected with two-tailed p-value ≤ 0.05 above its underlying background using the z-score test for difference of means.

III. Results

The results below show sample-uncorrelated background corrected spectra from each of the samples scanned except for Sample III, which was used to estimate background.

Fig. 3 and Fig. 4 show background corrected spectra from the benign and malignant tumor samples respectively. Several elements were identified common to both samples. Energy peaks were seen for Ag, Br, Cl, Co, Cr, Cs, Cu, Fe, Mg, Mn, Ni, Rb, Se, Sn, and Zn. Energy peaks were also seen for Ge from the gamma detectors. While several gamma energy peaks were seen to vary in intensity between the two samples, statistically significant differences were observed for the peaks listed in Table I. These peaks were found to correspond to Al, Br, Cl, Co, Fe, K, Rb and Zn.

Both breast samples were sent for spectral examination through neutron activation analysis (NAA). Results from the NAA indicated significant increases in the concentration of Cl, Fe, K, Na, and Zn and is shown in Table II.

Fig. 5 shows the gamma spectrum from the mixed Fe-Na-K-Cl sample containing 5 g Fe, 0.98 g Na, 1.31 g K, and 2.71 g Cl. Peaks were seen for each of the elements present in the sample. Assuming the statistical noise in the system to remain constant, the detection threshold for NSECT was calculated for each element and is shown in Table III.

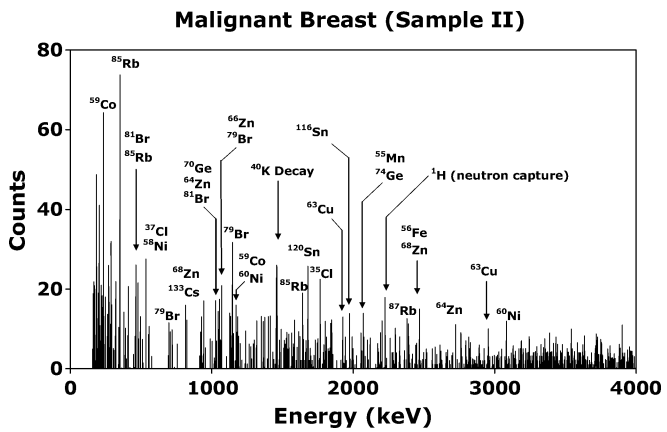

Fig. 4. Gamma energy spectrum from malignant breast sample showing energy peaks for several potential elements identified. Gamma peaks are seen for $^{72}\mathrm{Ge}$ and $^{74}\mathrm{Ge}$ from the germanium detector. Peaks with multiple potential element matches are labeled accordingly.

TABLE I
LIST OF ENERGY LEVELS SHOWING STATISTICALLY SIGNIFICANT DIFFERENCES IN INTENSITIES BETWEEN BENIGN AND MALIGNANT SPECTRA ALONG WITH A LIST OF POTENTIAL MATCHING ELEMENTS. ELEMENTS WITH NEGATIVE DIFFERENCES SHOWED A DECREASE IN CONCENTRATION IN THE MALIGNANT SAMPLE. THE STATISTICAL SIGNIFICANCE WAS CALCULATED USING A Z-SCORE TEST FOR DIFFERENCE OF MEANS

Energy keV	Element Match	Counts Benign	Counts Malignant	Diff	p-val
219	^{79}Br	6	19	13	0.01
397	^{59}Co, ^{79}Br	16	2	-14	0.01
1028	^{81}Br	13	29	16	0.05
1128	^{39}K, ^{68}Zn	0	13	13	0.001
1306	^{56}Fe	10	0	-10	0.01
2299	^{27}Al	0	13	13	0.001
2469	^{37}Cl, ^{56}Fe, ^{66}Zn	5	15	10	0.05
3635	^{35}Cl	3	14	11	0.01

TABLE II
LIST OF ELEMENTS SHOWING STATISTICALLY SIGNIFICANT DIFFERENCES IN CONCENTRATION BETWEEN BENIGN AND MALIGNANT TISSUE DETERMINED THROUGH NAA

Element	Cl	Fe	K	Na	Zn
Benign (µg/g)	2170	<172	<507	1440	3.96
Malignant (µg/g)	4000	902	834	3110	13.1

Fig. 6 shows the gamma energy spectrum accumulated for the fixed mouse specimen. Gamma peaks were observed for several elements expected from the mouse specimen as well as some from materials present in the scanning setup. Energy peaks were identified for $^{12}\mathrm{C}$ from tissue, $^{40}\mathrm{Ca}$ from bone, and elements $^{39}\mathrm{K}$, $^{27}\mathrm{Al}$, $^{37}\mathrm{Cl}$, $^{56}\mathrm{Fe}$, $^{68}\mathrm{Zn}$ and $^{25}\mathrm{Mg}$ which could be present in the specimen. Elements $^{27}\mathrm{Al}$ and $^{56}\mathrm{Fe}$ could also be system dependent as many components used to mount the detectors and other hardware were made of aluminum and iron. Peaks were seen for $^{158}\mathrm{Gd}$ and $^{160}\mathrm{Gd}$ from the 1:10 gadolinium/formalin fixing solution in the sample, along with peaks from several naturally occurring states in germanium in the HPGe detectors.

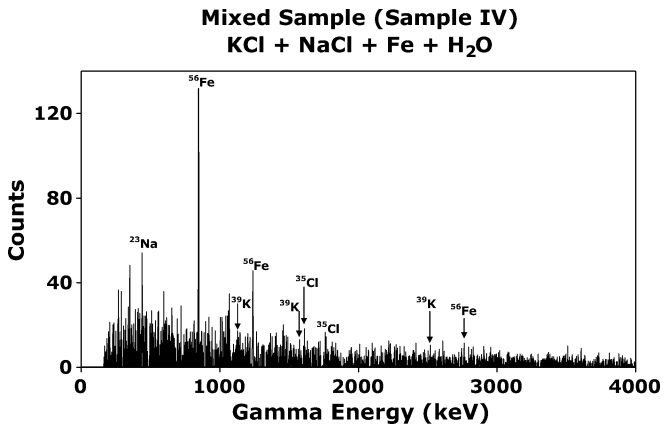

Fig. 5. Gamma energy spectrum from a mixed sample of 2.5 g KCl, 2.5 g NaCl and 5 g Fe in 40 g $\mathrm{H_2O}$. Peaks are seen for each of the elements in the sample.

TABLE III
RESULTS OF SENSITIVITY ANALYSIS FOR THE MULTI-ELEMENT CALIBRATION SAMPLE. ALSO LISTED FOR A COMPARATIVE ANALYSIS IS THE CORRESPONDING NAA SENSITIVITY FOR THE ELEMENT

	Mass	Peak	Threshold	Sensitivity	
	(g)	counts	counts	NSECT (g)	NAA (µg)
^{23}Na	0.98	140.21	40	0.28	5
^{56}Fe	5	519.79	72	0.69	90
^{39}K	1.31	71.47	32	0.59	1000
^{35}Cl	2.71	52.46	19	0.98	20

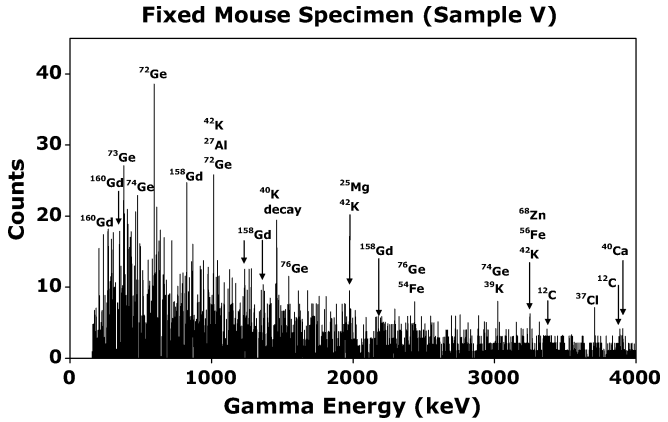

Fig. 6. Gamma energy spectrum from a formalin fixed mouse specimen showing peaks corresponding to excited states in various elements. Gamma peaks are seen for $^{12}\mathrm{C}$ (escape peaks), $^{40}\mathrm{Ca}$, $^{39}\mathrm{K}$, $^{27}\mathrm{Al}$, $^{37}\mathrm{Cl}$, $^{56}\mathrm{Fe}$, $^{68}\mathrm{Zn}$ and $^{25}\mathrm{Mg}$. Gamma peaks are also seen for $^{72}\mathrm{Ge}$ and $^{74}\mathrm{Ge}$ from the germanium detector, and $^{158}\mathrm{Gd}$ and $^{160}\mathrm{Gd}$ from the fixing solution. Peaks with multiple potential element matches are labeled accordingly.

IV. DISCUSSION

This work demonstrates that NSECT shows significant potential in developing into a modality capable of detecting breast cancer in early stages. Results from preliminary scans of breast tissue samples demonstrate its ability to detect individual elements within breast tissue. Energy peaks seen to vary in intensity between the benign and malignant samples facilitate future hypothesizing of these peaks as potential markers of breast cancer. Although the spectra obtained in this study were from

excised tissue, results from the whole mouse specimen indicate that element detection is possible for *in-vivo* tissue without the need for biopsy. The lower detection threshold for accurate quantification of an element using this preliminary NSECT system was found to range from 0.28 grams to 0.98 grams for the four elements analyzed. This threshold value is much higher than the microgram sensitivity required to detect cancer-indicating trace elements in the breast. Accurate element quantification using the current NSECT system requires at least the threshold concentration of the target element to be present in the beam. However, simulation experiments conducted to test the feasibility of breast cancer detection for *in-vivo* tumors have demonstrated the ability to detect microgram concentrations of trace elements that are markers of breast cancer for tumors that are *in-vivo* [36]. In some cases, it may be possible to increase the total mass of the element in the beam by using a broad neutron beam to illuminate a larger volume of the sample. Generally, a significant sensitivity improvement will be required in order to facilitate breast cancer diagnosis. Efforts are under way to improve sensitivity while maintaining the lowest possible dose level delivered to the patient. Using high-flux neutron sources and multiple gamma detectors will increase the overall detection efficiency and reduce scan time, which will both in turn reduce the time-dependent background noise. Optimizing the detector shielding will reduce the sample-related and room-related background, which will increase signal to noise ratio and improve the sensitivity of the system. Increasing the gamma detection efficiency to reduce overall scan time will also reduce the associated patient dose. Neutron and gamma attenuation correction algorithms are being developed and implemented simultaneously to improve sensitivity and detection accuracy [38].

Three background correction techniques were used in this experiment, TOF correction, sample-related background subtraction, and polynomial curve-fitting. The TOF correction technique is used to reduce the time-uncorrelated backgrounds. This background can also be estimated by acquiring a spectrum from a sample-out scan. Both techniques have been tested and are seen to suppress time-uncorrelated background sufficiently. We prefer to implement the TOF subtraction technique here because not only does it require less time by not having to acquire a separate sample-out scan, but the electronics are also readily available at TUNL. In a clinical environment however, it may be easier to use the sample-out subtraction technique to avoid the added complexity in required hardware.

Slowing and attenuation of neutrons in the body depends largely on the concentration of hydrogen and oxygen nuclei in the sample, and is of significant concern when interrogating large samples such as the abdomen. However, for the size of tumor samples that have been used in this study, simulations have shown that neutron slowing is not of significant concern. As larger samples are interrogated, neutron slowing and attenuation will be corrected in one of two ways: (a) Neutron energy slowing: Incident neutrons lose a part of their energy through interactions with nuclei encountered in the sample while traveling towards target trace element nuclei. As a result, the energy of the neutron available to interact with the target nucleus is lower. As the criterion for successful interrogation of a target nucleus through inelastic scatter spectroscopy is that the energy of the incident neutron must be larger than the target nuclear energy level to be excited, the reduction in energy through slowing of neutrons is taken into consideration when selecting the original incident energy of the neutron beam. For example, to interrogate a sample containing ^{12}C with its first excited state at 4.4 MeV, a 5 MeV neutron beam is used to ensure that there will be sufficient energy left to excite the 4.4 MeV energy state even after minor energy losses through slowing. (b) Neutron attenuation: Interactions such as elastic scatter between incident neutrons and nuclei encountered while traveling towards target trace elements often result in a change in direction of the incident neutron. As a result, fewer neutrons are able to reach the target trace element nucleus, leading to a reduction in the number of observed gamma counts for that nucleus. For spectroscopic examination of a homogeneous sample, this neutron attenuation is accounted for by using a calibration sample with the same geometric dimensions as the target tissue sample. For non-homogeneous samples which require tomographic examination, a neutron attenuation-correction algorithm has been developed for use with NSECT and has been described elsewhere [38].

Using neutrons as the incident radiation leads to significant concerns about patient dose. At our energies of interest (2 MeV to 8 MeV), neutrons are known to damage the body 10 times more than x-rays. However, as it takes fewer neutrons to create an NSECT image than x-rays required to create a mammogram, it is possible to maintain patient dose level at values comparable to other ionizing radiation modalities. In previous studies, it has been established that only 10,000 gamma events are required in the detectors to obtain quantitative accuracy of 95% in a tomographic image. Geant4 simulations to evaluate the efficiency of inelastic scatter interactions have shown that 10,000 gamma events can be obtained in the detectors using 10 million incident neutrons, which corresponds to an effective patient dose of less than 1 mSv. Our preliminary simulation experiments suggest that for breast cancer detection, it may be possible to achieve effective patient dose levels lower than 5 mSv [36], [39]. By increasing the number of detectors and using high-flux neutron sources to reduce scan time, dose levels can potentially be brought down even further. Dose assessments are currently performed through a Geant4 simulation which models the acquisition geometry, neutron beam characteristics and tissue sample data [39]. The simulation is used to count the energy deposited in the tissue sample from which an effective dose equivalent for the organ can be calculated by using the appropriate weighting factors for the organ of interest. For the breast, the weighting factor relative to whole body exposure is 0.05.

An important issue to address for breast cancer diagnosis using NSECT is the accurate quantification of a particular element in the spectrum despite line contributions to its gamma peaks from other elements. This involves an understanding of the nuclear transition structure of the element under evaluation, and subsequent correction for the 'noise' line-contributions from other elements. These line contributions have been evaluated experimentally for several samples. Before quantification experiments can be performed for micro-gram concentrations of breast trace elements, it is imperative to analyze the line contributions from each of the elements of interest and develop a model to identify an element based on its gamma line contributions throughout the spectrum. Efforts are under way to evaluate gamma spectra from several such elements using Geant4 simulation.

NSECT is a new alternate diagnosis method with the potential to detect breast cancer. Its advantage lies in its ability to detect and identify malignant tissue in the breast and generate a two-dimensional image through a single non-invasive *in-vivo* tomographic scan without the need for breast compression or biopsy. Through the use of portable neutron sources and portable gamma detectors, NSECT can potentially be translated to clinical use as a screening and diagnostic technique for breast cancer. Our final goal is to implement a portable, low-dose breast cancer screening system which can detect breast cancer without the need for breast compression or invasive biopsies.

ACKNOWLEDGMENT

The authors thank all the members of the Triangle Universities Nuclear Laboratory for their help with data acquisition and the members of the Duke Advanced Imaging Laboratories for their help with data analysis. They also thank the Center for In-vivo Microscopy at Duke University for providing the fixed mouse specimen.

REFERENCES

[1] A. Garg and V. Singh *et al.*, "An elemental correlation study in cancerous and normal breast tissue with successive clinical stages by neutron activation analysis," *Biol. Trace Element Res.*, vol. 46, pp. 185–202, 1994.

[2] Y. Katoh, T. Sato, and Y. Yamamoto, "Use of instrumental neutron activation analysis to determine concentrations of multiple trace elements in human organs," *Arch. Environ. Health*, Oct. 2003.

[3] G. S. Knight, A. H. Beddoe, S. J. Streat, and G. L. Hill, "Body composition of two human cadavers by neutron activation and chemical analysis," *Am. J Physiol. Endocrinol. Metab.*, vol. 250, pp. E179–E185, 1986.

[4] M. Yukawa, M. Suzuki-Yasumoto, K. Amano, and M. Terai, "Distribution of trace elements in the human body determined by neutron activation analysis," *Arch. Environ. Health*, vol. 35, pp. 36–44, 1980.

[5] A. Danielsen and E. Steinnes, "A study of some selected trace elements in normal and cancerous tissue by neutron activation analysis," *J. Nucl. Med.*, vol. 11, pp. 260–264, 1970.

[6] K. H. Ng, D. A. Bradley, L. M. Looi, C. Seman Mahmood, and A. Khalik Wood, "Differentiation of elemental composition of normal and malignant breast tissue by instrumental neutron activation analysis," *Appl. Radiat. Isot.*, vol. 44, pp. 511–516, 1993.

[7] G. V. Iyengar, K. Kasperek, and L. E. Feinendegen, "Determination of certain bulk and trace elements in the bovine liver matrix using neutron activation analysis," *Phys. Med. Biol.*, vol. 23, pp. 66–76, 1978.

[8] W. E. Kollmer, P. Schramel, and K. Samsal, "Simultaneous determination of nine elements in some tissues of the rat using neutron activation analysis," *Phys. Med. Biol.*, vol. 17, pp. 555–562, 1972.

[9] C. E. Floyd, J. E. Bender, A. C. Sharma, A. J. Kapadia, J. Q. Xia, B. P. Harrawood, G. D. Tourassi, J. Y. Lo, A. S. Crowell, and C. R. Howell, "Introduction to neutron stimulated emission computed tomography," *Phys. Med. Biol.*, vol. 51, pp. 3375–3390, 2006.

[10] C. E. Floyd, A. J. Kapadia, J. E. Bender, A. C. Sharma, J. Q. Xia, B. P. Harrawood, G. D. Tourassi, J. Y. Lo, A. S. Crowell, and C. R. Howell, "Neutron stimulated emission computed tomography of a multi-element phantom," *Phys. Med. Biol.*, submitted for publication.

[11] C. E. Floyd, C. R. Howell, B. P. Harrawood, A. S. Crowell, A. J. Kapadia, R. Macri, J. Q. Xia, R. Pedroni, J. Bowsher, M. R. Kiser, G. D. Tourassi, W. Tornow, and R. Walter, "Neutron stimulated emission computed tomography of stable isotopes," in *Proc. SPIE Medical Imaging 2004*, vol. 5368, pp. 248–254.

[12] A. J. Kapadia, C. E. Floyd, J. E. Bender, C. R. Howell, A. S. Crowell, and M. R. Kiser, "Non-invasive quantification of iron 56-Fe in beef liver using neutron stimulated emission computed tomography," in *Proc. IEEE Nuclear Science Symp., Medical Imaging Conf. 2005*, vol. 4, pp. 2232–2234.

[13] A. J. Kapadia, A. C. Sharma, G. D. Tourassi, J. E. Bender, A. S. Crowell, M. R. Kiser, C. R. Howell, and C. E. Floyd, "Neutron spectroscopy of mouse using Neutron Stimulated Emission Computed Tomography (NSECT)," in *Proc. IEEE Nuclear Science Symp., Medical Imaging Conf. 2006*, vol. 6, pp. 3546–3548.

[14] A. J. Kapadia, A. C. Sharma, G. D. Tourassi, J. E. Bender, A. S. Crowell, M. R. Kiser, C. R. Howell, and C. E. Floyd, "Neutron Stimulated Emission Computed Tomography (NSECT) for early detection of breast cancer," in *Proc. IEEE Nuclear Science Symp., Medical Imaging Conf. 2006*, vol. 6, pp. 3928–3931.

[15] A. J. Kapadia, A. C. Sharma, G. D. Tourassi, J. E. Bender, A. S. Crowell, M. R. Kiser, C. R. Howell, and C. E. Floyd, "Non-invasive estimation of potassium (39K) in bovine liver using Neutron Stimulated Emission Computed Tomography (NSECT)," in *Proc. IEEE Nuclear Science Symp., Medical Imaging Conf. 2006*, vol. 4, pp. 2076–2078.

[16] J. E. Bender, C. E. Floyd, B. P. Harrawood, A. J. Kapadia, A. C. Sharma, and J. L. Jesneck, "The effect of detector resolution for quantitative analysis of neutron stimulated emission computed tomography," in *Proc. SPIE Medical Imaging 2006*, vol. 6142, pp. 1597–1605.

[17] A. C. Sharma, G. D. Tourassi, A. J. Kapadia, J. E. Bender, J. Q. Xia, B. P. Harrawood, A. S. Crowell, M. R. Kiser, C. R. Howell, and C. E. Floyd, "Development of a high-energy gamma camera for use with NSECT imaging of the breast," in *Proc. IEEE Nuclear Science Symp., Medical Imaging Conf. 2006*, vol. 6, pp. 3925–3927.

[18] K. H. Ng, D. A. Bradley, and L. M. Looi, "Elevated trace element concentrations in malignant breast tissues," *Brit. J. Radiol.*, vol. 70, pp. 375–382, 1997.

[19] S. Rizk and H. Sky-Peck, "Comparison between concentrations of trace elements in normal and neoplastic human breast tissue," *Cancer Res.*, vol. 44, pp. 5390–5394, 1984.

[20] A. Schwartz and R. Fink, "Trace elements in normal and malignant human breast tissue," *Surgery*, vol. 76, pp. 325–329, 1974.

[21] R. Engelhardt, J. H. Langkowski, R. Fischer, P. Nielsen, H. Kooijman, H. C. Heinrich, and E. Bucheler, "Liver iron quantification: Studies in aqueous iron solutions, iron overloaded rats, and patients with hereditary hemochromatosis," *Magn. Reson. Imaging*, vol. 12, pp. 999–1007, 1994.

[22] J. P. Villeneuve, M. Bilodeau, R. Lepage, J. Cote, and M. Lefebvre, "Variability in hepatic iron concentration measurement from needle-biopsy specimens," *J. Hepatol.*, vol. 25, pp. 172–177, 1996.

[23] J. M. Alustiza, J. Artetxe, A. Castiella, C. Agirre, J. I. Emparanza, P. Otazua, M. Garcia-Bengoechea, J. Barrio, F. Mujica, and J. A. Recondo, "MR quantification of hepatic iron concentration," *Radiology*, vol. 230, pp. 479–484, 2004.

[24] L. W. Powell, "Diagnosis of hemochromatosis," *Semin. Gastrointest. Dis.*, vol. 13, pp. 80–88, 2002.

[25] S. R. Hollan, "Transfusion-associated iron overload," *Curr. Opin. Hematol.*, vol. 4, pp. 436–441, 1997.

[26] S. Joffe, "*Hemochromatosis*" [Online]. Available: http://www.emedicine.com/radio/topic323.htm 2005

[27] L. Powell, "Hemochromatosis," in *Harrison's Principles of Internal Medicine*, D. Kasper, A. S. Fawci, D. L. Longo, E. Braunwald, S. L. Hauser, and J. L. Jameson, Eds., 16th ed. New York: McGraw Hill, 2005, vol. 2, pp. 2298–2303.

[28] G. Brewer, "Wilson disease," in *Harrison's Principals of Internal Medicine*, D. Kasper, A. S. Fawci, D. L. Longo, E. Braunwald, S. L. Hauser, and J. L. Jameson, Eds., 16th ed. New York: McGraw Hill, 2005, vol. 2, pp. 2313–2315.

[29] A. P. Dempster, N. M. Laird, and D. B. Rubin, "Maximum likelihood from incomplete data via the EM algorithm," *J. Royal Stat. Soc. Series B*, vol. 39, pp. 1–38, 1977.

[30] R. Sundberg, "Maximum likelihood theory for incomplete data from an exponential family," *Scand. J. Stat.*, vol. 1, pp. 49–58, 1974.

[31] L. Shepp and Y. Vardi, "Maximum likelihood reconstruction for emission tomography," *IEEE Trans. Med. Imag.*, vol. MI-1, pp. 113–122, Oct. 1982.

[32] H. Mussalo-Rauhamaa, S. Piepponen, J. Lehto, R. Kauppila, and O. Auvinen, "Cu, Zn, Se and Mg concentrations in breast fat of Finnish breast cancer patients and healthy controls," *Trace Elements in Med.*, vol. 10, pp. 13–15, 1993.

[33] C. R. Howell and Q. Chen *et al.*, "Toward a resolution of the neutron-neutron scattering length issue," *Phys. Lett. B*, vol. 444, pp. 252–259, 1998.

[34] P. Håkansson, "An introduction to the time-of-flight technique," *Braz. J. Phys.*, vol. 29, pp. 422–427, 1999.

[35] C. E. Floyd, A. C. Sharma, J. E. Bender, A. J. Kapadia, J. Q. Xia, B. P. Harrawood, G. D. Tourassi, J. Y. Lo, M. R. Kiser, A. S. Crowell, R. S. Pedroni, R. A. Macri, S. Tajima, and C. R. Howell, "Neutron stimulated emission computed tomography: Background corrections," *Nucl. Instrum. Methods Phys. Res. Section B*, vol. 254, pp. 329–336, 2007.

[36] J. E. Bender, A. J. Kapadia, A. C. Sharma, G. D. Tourassi, B. P. Harrawood, and C. E. Floyd, "Breast cancer detection using neutron stimulated emission computed tomography: Prominent elements and dose requirements," *Med. Phys.*, vol. 34, pp. 3866–3871, 2007.

[37] National Nuclear Data Center BNL, NuDat 2.3 2007.

[38] A. J. Kapadia and C. E. Floyd, "An attenuation correction technique to correct for neutron and gamma attenuation in the reconstructed image of a neutron stimulated emission computed tomography (NSECT) system," in *Proc. SPIE Medical Imaging 2005*, vol. 5745, pp. 737–743.

[39] A. C. Sharma, B. P. Harrawood, A. J. Kapadia, J. E. Bender, and G. D. Tourassi, "Neutron stimulated emission computed tomography: A Monte Carlo simulation approach," *Phys. Med. Biol.*, vol. 52, pp. 6117–6131, 2007.